Viscoelastic Analysis of Surface Responses in Flexible Pavements under Different Loading Conditions

Mohsen Alae[1]; Zhen Leng[2]; Yanqing Zhao[3]; Guozhi Fu[4]

[1]Research Assistant, School of Transportation Engineering, Dalian University of Technology, Dalian 116024, China. Email: mohsen_374@yahoo.com

[2]Associate Professor, Department of Civil and Environmental Engineering, The Hong Kong Polytechnic University, Hung Hom, Kowloon, Hong Kong. Email: zhen.leng@polyu.edu.hk

[3]Professor, School of Transportation Engineering, Dalian University of Technology, Dalian 116024, China. Email (corresponding author): yanqing_zhao@dlut.edu.cn

[4]Research Assistant, School of Transportation Engineering, Dalian University of Technology, Dalian 116024, China. Email: fuguozhi@mail.dlut.edu.cn

Abstract: Due to time-temperature dependent behavior of asphalt concrete (AC), viscoelastic analysis is necessary for understanding the mechanism of top-down cracking (TDC). In this study, a new approach for determining the viscoelastic surface responses of multilayered asphalt pavements was developed to solve the complicated oscillating behavior and slow convergence of the integrand of Laplace-transformed step-response function at the pavement surface. By employing the Lucas algorithm, the irregular oscillations were reduced to regular oscillations by separating the integrand into high- and low-frequency components. After that, the integration, summation, and extrapolation approaches were applied to converge the variations. The results calculated from the proposed approach were widely verified against finite-element (FE) results. According to horizontal strains calculated at pavement surface, mechanism of TDC initiation was investigated under stationary and moving loads. The results indicated that high temperature and low vehicle speed were among the predominant factors contributing to TDC initiation. In addition, TDCs were more likely to initiate at a very close distance to the tire edge. The method proposed in this study provides a valuable tool for accurately determining the viscoelastic surface response of asphalt pavements.

Keywords: viscoelastic analysis; top-down cracking; moving load; horizontal strain; asphalt pavement

1. Introduction

A pavement structure experiences various damages and distresses within its service life due to the traffic and temperature impacts. In recent years, longitudinal top-down cracking (TDC) in asphalt concrete (AC) has increased researchers' attention for investigating the primary mechanism of this distress. TDC is a load-induced fatigue cracking, which appears at the proximity of wheel path and propagates downward (Wang et al., 2013; Dinegdae and Birgisson, 2018; Gu et al., 2018; Alae et al., 2020). By developing calibrated mechanistic-empirical (M-E) models, TDC performance has been explored with actual traffic load and thermal stress (Dinegdae et al., 2015; Ling et al., 2019; Wu and Muhunthan, 2019a). Several studies revealed that some factors such as environmental conditions, tire–pavement contact stress, and interface bonding conditions affect pavement responses and can be related to TDC initiation (Wang and Al-Qadi, 2010; Grellet et al., 2018).

Since the flexible pavements are horizontally layered, Burmister (1945) proposed analytical layered elastic models to compute stress and strain responses. Using Richardson's extrapolation, Maina and Matsui (2005) have calculated the elastic responses at the top of pavement and demonstrated that the approach employed can enhance the accuracy of elastic responses. However, the responses calculated at the surface show differences with boundary conditions at tire edge. In order to enhance the surface response convergence, an elastic analysis approach was proposed to compute the discrepancies between the original system and that of a half-space with similar surface layer properties (Khazanovich and Wang, 2007). It is well-recognized that asphalt mixture behavior is time and temperature dependent, and linear elastic assumption for AC layer may result in inaccurate results. Therefore, viscoelastic response analysis is essential for evaluating the pavement performance and identifying TDC mechanism.

Various semi-analytical software such as, VEROAD, 3D-Move, and ViscoRoute have been developed to simulate the moving load effects on asphalt pavement (Nilsson et al., 1996; Chabot et al., 2010; ARC, 2013). The results obtained from the semi-analytical method demonstrated that it is necessary to incorporate viscoelastic effects in the modeling to predict pavement behavior well and anticipate possible damages in the structure. The finite element method (FEM) has been extensively employed to perform viscoelastic analysis for various distresses over the last decade (Elseifi et al., 2006; Dubois et al., 2012). But, a complete implementation of FEM for the pavement with numerous sublayers and loading types seems to be time-consuming for routine design. Chen et al. (2009) utilized an approach which is called dual parameter for computing the viscoelastic responses, because AC material can be characterized by Prony series expressions of both the creep compliance and relaxation modulus. Furthermore, a new model based on viscoelastic continuum damage (VECD) mechanics has been developed for exploring crack initiation in NCHRP 01-42A study (Roque et al., 2010).

Nevertheless, these efforts did not lead to the accurate determination of TDC. For example, the results indicated that the base layer stiffness does not affect the likelihood of TDC initiation, which contradicts the field observation (Wu et al., 2019b).

Once the pavement is subjected to complex loading and environmental conditions, viscoelastic responses are significantly influenced by current and previous inputs. Loading frequency is a critical factor in time-dependent materials which accelerate the fatigue failure in asphalt pavement (Qin et al., 2010; Rahman et al., 2018). Field investigations revealed that the vehicle speed reduction intensifies the critical strain at the bottom and middle of asphalt layer exponentially (Dai et al., 1997). In the research conducted by Alae et al. (2019), high loading frequency influence on TDC propagation was similar to low temperature, at different distances from the tire edge.

The AC layer experiences a wide range of temperatures within its depth due to the variation of air temperature. Also, the temperature at the bottom of AC layer requires a longer time to alter compared to that at the surface. Hence, considering non-uniform temperature gradients is essential in the viscoelastic analysis of TDC. Archilla (2015) utilized the inverse modulus gradient in thick pavements, and figured out high temperature increases possibility of TDC initiation significantly. To evaluate the effects of these critical factors on viscoelastic responses at the surface, TDC mechanism should be known.

Horizontal shear stress in the tire–pavement interface and vertical shear strain at the tire edge in thick AC layer have been identified as the mechanisms for development of TDC (Groenendijk, 2000; Wang, 2011). In contrast, Myers et al., (2001) noted that a radial tire causes large tensile stress at the tire–pavement interaction, which is significant in explanation of TDC mechanism. Moreover, the newly mechanistic-empirical pavement design guide (MEPDG) recommended that horizontal tensile strain is a critical parameter for surface- initiated cracking (ARA, 2004). According to this finding, researchers have made notable efforts to develop new M-E models in a compatible procedure with MEPDG approach (Wu et al., 2019a; Ling et al., 2020). It was also demonstrated that the method used in MEPDG for calculation of maximum tensile strain at the surface may result in inaccurate TDC prediction because of inadequate analysis points around the tire edge (Alae et al. 2020).

Accurate determination of pavement response at the surface plays an important role to efficiently model the top-down cracking. However, the surface viscoelastic solution in the transformed domain shows slow convergence and complicated oscillating behavior, the primary objective of this study was to develop a viscoelastic analysis procedure to effectively solve this issue and compute the horizontal strains at the pavement surface. The accuracy of the method employed in this study were extensively verified with FE results. The results were calculated under stationary and moving loads at various loading frequencies and temperatures, in which the moving load responses were computed based on the superposition procedure. By identifying the critical location of TDC from viscoelastic analysis, the results were compared with those adopted in MEPDG. The approach employed in this study can provide valuable insight into pavement analysis and design from M-E point of view.

2. Methodology

2.1. Elastic Solution for Layered Systems

Layered elastic models assume that each pavement structural layer is homogeneous, isotropic, and linearly elastic. The bottom layer is an infinite half-space and materials are not stressed beyond their elastic ranges. To characterize a pavement response effectively, elastic modulus and Poisson's ratio of each layer, Pavement layer thicknesses and loading conditions are required. The outputs of a layered elastic model are the stresses, strains, and deflections in the pavement. Once a pavement is subjected to a uniform circular load with radius a and pressure magnitude q, the elastic solution can be analytically derived from the layered elastic theory. For instance, Burmister's solution for the horizontal radial stress in the ith layer is given by (Burmister 1943; Huang 2003):

$$R = q\alpha\int_0^{\infty}\left[J_0(m\rho)J_1(m\alpha)-\frac{J_1(m\rho)J_1(m\alpha)}{m\rho}\right]\left\{\begin{array}{l}\left[A_i+C_i(1+m\lambda)\right]e^{-m(\lambda_i-\lambda)}\\+\left[B_i-D_i(1-m\lambda)\right]e^{-m(\lambda-\lambda_{i-1})}\\+2\mu_i m J_0(m\rho)\left[C_i e^{-m(\lambda_i-\lambda)}-D_i e^{-m(\lambda-\lambda_{i-1})}\right]\end{array}\right\}dm \quad (1)$$

where $\rho = {r}/{H}$ and $\lambda = {z}/{H}$; H is the distance from the surface to the upper boundary of the lowest layer; r and z are the cylindrical coordinates in radial and vertical directions; m is a parameter; J_0 and J_1 are Bessel functions of the first kind and order of zero and one, respectively. A_i, B_i, C_i, and D_i are constants of integration of the ith layer. These constants are determined from the boundary and continuity conditions. α is the ratio of load radius to H and q is the load magnitude.

2.2. Viscoelastic Solution Derivation

The assumption made in the layered elastic theory that AC is linear elastic simplifies the analysis, but may cause inaccurate results. In this study, the derivation of viscoelastic solution for multilayered pavement structure was based on elastic-viscoelastic correspondence principle (EVECP). The set of Laplace-transformed governing equations of a viscoelastic boundary-value problem (BVP) constituted an associated elastic problem (Haddad 1995). According to correspondence principle, if an elastic solution to a BVP is known, substitution of the appropriate Laplace transforms of the quantities utilized in the elastic analysis furnishes the viscoelastic solution in the transform plane. The time-domain response was solved through numerical transform inversion and was then expressed in form of an exponential series with the relationship between the exponential series coefficients and the step responses at zero and infinite time.

The constitutive relationship of linear viscoelastic (LVE) materials described in the Laplace domain was shown in Equation (2) (Tschoegl 1989).

$$\bar{\sigma}(s) = \bar{Q}(s)\bar{\varepsilon}(s) \quad (2)$$

where $\bar{\sigma}(s)$ and $\bar{\varepsilon}(s)$ were Laplace transforms of stress and stain histories, respectively; s was Laplace variable; and $\bar{Q}(s)$ was material relaxation. A bar over a symbol indicates the quantity was transformed into Laplace.

The relaxation was the Laplace conversion of the impulse response function, which was a material response to the unit impulse strain input represented by a delta function. In the linear time-invariant system theory, $\bar{Q}(s)$ also denotes the transfer function and delta function is a mathematical abstraction. To determine the viscoelastic solution in the Laplace domain, the Young's modulus utilized in the elastic analysis was substituted by the relaxation of the material according to the correspondence principle. To obtain relaxation of LVE materials, the theoretical relationship given by Equation (3) was employed (Tschoegl 1989).

$$\bar{Q}(s) = E^*(i\omega)|_{\,i\omega=s} \quad (3)$$

where $E^*(i\omega)$ is complex modulus; ω is angular frequency and $i = \sqrt{-1}$. By substituting $i\omega$ in $E^*(i\omega)$ with the Laplace variable (s), the viscoelastic materials relaxation was simply determined. It was shown in the "Material Characterization" section, the model presented was efficient in characterizing AC behavior in the complex domain. The Poisson's ratio was another material parameter, which is usually assumed to be time independent for asphalt mixtures (Al-Qadi and Wang, 2009; Elseifi et al., 2006).

To evaluate the viscoelastic response of pavement structure subjected to an arbitrary or moving load, the step response function was calculated. The step response function, $R_H(t)$, is the pavement response to a unit step loading history, obtained as follows:

$$P(t) = \begin{cases} 1 \text{ MPa}, & \mathrm{t} \geq 0 \\ 0 \text{ MPa}, & \mathrm{t} < 0 \end{cases} \tag{4}$$

the Laplace transform of $P(t)$ in the equation is *1/s*.

2.3. Laplace Transform Inversion

In the Laplace domain, viscoelastic step response function was determined by substituting the relaxation and Laplace transform of the applied load into the elastic solution. Due to the complexity of the analytical inversion transform, the numerical Laplace transform inversion in the time domain was used in the analysis. Among various methods introduced for numerical Laplace inversion, Gaver functional was the most powerful and proven method which was written as below (Gaver, 1966; Valkó and Abate, 2004; Zhao et al., 2014):

$$f_k(t) = k\tau \binom{2k}{k} \sum_{j=0}^{k} (-1)^j \binom{k}{j} \bar{f}[(k+j)\tau] \tag{5}$$

where $\tau = \ln(2)/t$. To increase the accuracy of Gaver functional, the Wynn's Rho algorithm was used as an acceleration scheme which was given by following formulations (Valkó and Abate, 2004; Guo et al., 2020):

$$\rho_{-1}^{(n)} = 0, \quad \rho_0^{(n)} = f_n(t), \qquad 0 \leq n \leq 2m \tag{6a}$$

$$\rho_k^{(n)} = \rho_{k-2}^{(n+1)} + \frac{k}{\rho_{k-1}^{(n+1)} - \rho_{k-1}^{(n)}}, \qquad 1 \le k \le 2m\,, 0 \le n \le 2m-k \qquad (6b)$$

the time-domain function was obtained as:

$$f(t_i) = \rho_{2m}^{(0)} \qquad (7)$$

where *f(t$_i$)* is the final solution in time domain; t_i is the *i*th analysis time; and *m* is the parameter that determines the accuracy of Laplace inversion. In this study, utilizing Gaver-Wynn-Rho (GWR) algorithm illustrated in Equations (5) to (7), the Laplace transform was inverted numerically.

It is significant to note that, there were difficulties in determining surface viscoelastic responses due to the irregular oscillations caused by the product of two Bessel functions $(J_0\,, J_1)$ in Laplace transform of the step-response function in Equation (8).

$$\overline{R_H}(s) = \frac{\alpha p_0}{s}\int_0^\infty \bar{F}(m,s)dm = \frac{\alpha p_0}{s}\int_0^\infty \bar{f}(m,s)J_0(\rho m)J_1(\alpha m)\,dm \qquad (8)$$

The value of $\bar{f}(m,s)$ denotes the Laplace transformed response of stresses or displacements. To identify the difficulties in determining surface responses, the behavior of the integrand, $\bar{F}(m,s)$, was explored. A typical pavement structure at two points (A and B), was analyzed. Both points were at a radial distance of 6 cm from the loading center. Point A was at pavement surface, whereas Point B was at 10 cm below the surface. The value of $\bar{F}(m,s)$ was obtained at various *m* values and a fixed *s* value of 1.73 + 1.26*i*, which was one of the Laplace points, for a time of 1 second. Figures 1(*a* and *b*) showed the real and imaginary parts of $\bar{F}(m,s)$ for vertical stress at Points A and B, respectively.

The results clearly showed that difficulties involved in the determination of surface viscoelastic response. Unlike the response at Point B, the integrand showed oscillatory behavior at the surface (Point A) and approached zero at large m values. This complicated oscillating behavior implies that responses at the surface may not be calculated accurately. In the next step, in order to overcome this problem, the algorithm introduced by Lucas (1995) was employed to separate the integrand in equation above as the sum of two oscillating functions.

$$\overline{R_H}(s) = \frac{\alpha p_0}{s}\left[\int_0^{\infty} \bar{f}(m,s)h_1(m)\,dm + \int_0^{\infty} \bar{f}(m,s)h_2(m)\,dm\right] \tag{9}$$

The h_1 represents the high-frequency components, while h_2 shows low-frequency component. Utilizing integration, summation, and then extrapolation (ISE) approach, the real and imaginary parts of the high- and low-frequency component for Point A were calculated, and the results were shown in Figures 2(a and b), respectively. It can be seen that complicated oscillating behavior of $\bar{F}(m,s)$, as shown in Figure 1a has been converted to regular oscillations. To compute the time-domain viscoelastic response, the procedure in a computer code was developed to implement the EVECP.

2.4. Responses to Arbitrary and Moving Loads

A pavement, including linear elastic and viscoelastic layers, was considered a linear system, and Boltzmann superposition principle was employed to compute the responses as a result of arbitrary and moving loads. When the step response function was available, viscoelastic responses were calculated based on convolution integral, which was as follows:

$$O(t) = \int_0^t R_H(t-\tau)\frac{\partial I(\tau)}{\partial \tau}\,d\tau \tag{10}$$

where $R_H(t)$ is step response function; $O(t)$ is output viscoelastic response; $I(t)$ is input loading history; τ is integral variable.

The responses under arbitrary load histories were investigated by utilizing the haversine load applied to a fixed area on the pavement surface. The haversine loading history was written as below:

$$P(t) = A\left[\frac{1}{2} + \frac{1}{2}sin\left(\frac{2\pi t}{d} - \frac{\pi}{2}\right)\right] \tag{11}$$

where A is tire pressure amplitude in MPa; d is duration of load in second which is equal to $12a/V$; V is speed of moving load in m/s; and a is radius of contact area in meter.

To conduct the moving load analysis at different speeds, the path of moving load was divided into small elements with equal length, and a discrete formulation of the Boltzmann superposition principle was obtained. For the problem in hand, the formulation was simplified because the loading area was treated as one element. Moreover, the load movement was assumed along the traffic direction at each shift, while the load amplitude represented by haversine function in Equation (11) was applied to each loading area. The moving load equation was as follow:

$$R(t) = \sum_{i=1}^{N} p_i R_H(x_0 - d_i, y_0, z_0, t - t_i) \tag{12}$$

where $R(t)$ is viscoelastic response; N is number of shifts, where the first shift is at zero time; x_0, y_0, and z_0 are distances between the load center and analysis point at zero time in x-, y-, and z-directions, respectively; d_i is distance along which the load moves in the x direction at the ith shift; p_i is load pressure applied at the ith shift; and t_i is time at which the load moves to ith shift. When the load moves from shift i to $i + 1$, a pressure p_{i+1} was applied at location $i + 1$, and simultaneously a pressure p_i was unloaded at location i, which was equivalent to applying a negative p_i at location i. Hence, the step response function was evaluated at $x_0 - d_{i+1}$ and $x_0 - d_i$ for loading and unloading, respectively.

2.5. Material Characterization

The relaxation of LVE materials is in correlation with complex modulus. Using the Modified Havriliak-Negami (MHN) model in this research, behavior of AC was characterized in complex domain. The MHN model was given by (Zhao et al., 2014):

$$E^*(i\omega_r) = E_0^* + \frac{E_\infty^* - E_0^*}{\left[1+(\frac{\omega_0}{i\omega_r})^\alpha\right]^\beta} \tag{13}$$

where ω_r is reduced angular frequency; E_∞^* and E_0^* are complex moduli as ω_r approaches ∞ and 0, respectively; ω_0 is related to the time-temperature shifting and controls the horizontal positions of master curves, and α and β are model coefficients. According to the time-temperature superposition principle (TTSP), ω_r and cyclic frequency, f, were related by (Ferry, 1980):

$$\omega_r = 2\pi f \alpha_T \tag{14}$$

where α_T is the time-temperature shift factor. The Williams-Landel-Ferry (WLF) equation was used to model α_T as a function of temperature T:

$$\log \alpha_T = \frac{-C_1(T-T_0)}{C_2+(T-T_0)} \tag{15}$$

where C_1 and C_2 are model coefficients and T_0 is the reference temperature.

In this study, hot mix asphalt (HMA) with the maximum aggregate size of 19 mm and an SBS-modified PG 76-22 binder was utilized to conduct dynamic modulus test at six frequencies (20, 10, 5, 1, 0.5 and 0.1 Hz) and six temperatures (-10, 0, 15, 30, 40 and 55°C). By fitting dynamic modulus data with the sigmoidal function, and utilizing a nonlinear minimization algorithm, the sigmoidal function coefficients were computed at reference temperature 25°C as presented in Table 1. Once the complex modulus was calculated, the relaxation of AC was obtained from Equation (3).

The typical pavement structure parameters shown in Table 2 were considered for computing the viscoelastic responses at the top and bottom of AC layers under stationary and moving loads. Since the viscoelastic behavior of AC mixtures is highly dependent on pavement temperature, the horizontal strains were computed at 5, 25 and 50°C. These temperatures were considered at the pavement surface in the analyses, whereas the positive and negative temperature gradients were assumed for high and low temperatures within the AC layer depth. By dividing the AC layer to sublayers with 2 cm thickness and introducing a rate of linear temperature differential of 1.1ºC/cm based on previous studies (Wang, 2011; Sangpetngam et al., 2004), the corresponding temperatures were determined in various depths of AC layer. Figure 3 depicted the temperatures gradients in a thick AC layer.

Moreover, the circular uniform dual tires loading with a pressure of 0.7 MPa and a diameter of 20 cm was considered in the analyses, whereas the center-to-center distance of the dual tires was 30 cm.

2.6. Verification of Solutions against FEM Results

In this section, viscoelastic responses from the proposed approach were verified against the FEM results. Analyses were conducted at reference temperature 25°C on a typical pavement structure with 20 and 40 cm thicknesses for AC and base layer, respectively. While the viscoelastic modulus of AC layer was determined from MHN model, the elastic moduli of base layer and subgrade were assumed 300 and 80 MPa, respectively. In addition, the corresponding Poison’s ratios were considered 0.3, 0.35 and 0.4. Using the axisymmetric models, FE analyses were performed by the software ABAQUS 6.14. To minimize the edge effect errors, the model dimensions in horizontal and vertical directions were selected 5 m. Four-node quadrilateral elements were considered in modeling, with fine mesh near the loading area and pavement surface and relatively coarse mesh farther away from the loading area. While the bottom of the model was fixed on both horizontal and vertical directions, a roller support was employed for the right side (Saad et al. 2005).

Two points at the pavement surface with radial distances of 0 and 13 cm from the loading center were investigated. Figure 4 represented the displacements calculated under the loading center (0 cm) and at a radial distance of 13cm from the proposed approach match well with those computed from FEM analyses. In addition, comparisons of horizontal stresses computed from the proposed approach and FEM were illustrated in Figures 5(*a* and *b*) under the center of the tire and at a radial distance of 13 cm, respectively. The results showed that the proposed approach could accurately determine the viscoelastic responses at the pavement surface.

Under a haversine loading, the surface horizontal stresses at the center of the tire load from the proposed approach were compared with those calculated from FEM and the results were shown in Figure 6. According to Equation (11), the values of load duration (d) and pressure amplitude (A) were assumed 0.1 second and 0.7 MPa, respectively. The results obtained from two approaches were in good agreement, and the proposed procedure in this research decreased the computation time significantly. Using a computer with Intel i5 CPU, analysis time of the proposed approach was 23 seconds, while it was 17 minutes for the FEM. The results showed that the method introduced in this study accurately calculated viscoelastic surface responses.

3. Results and Discussions

To identify the critical horizontal strain locations in pavements with CTB and GB layers, 28 transverse locations were analyzed for defining the response profiles. Because of the symmetric boundary conditions at the center of dual tires, the horizontal strain profiles were only shown from the middle point of dual tires to a distance of 55 cm. The sketch of 3D pavement structure with the contact area and analysis points were depicted in Figure 7.

3.1. Stationary Load Effect on Horizontal Strains

3.1.1. Pavements with Cement-Treated Base

The viscoelastic strain profiles of a thick AC layer at three temperatures (5°C, 25°C and 50°C) were demonstrated in Figures 8(*a, b* and *c*) for the pavements with CTB layer. The figures showed that the longitudinal strains (ε_y) at the bottom of AC layer were in compression due to the negative values. But the transverse strains (ε_x) at the top indicated different patterns.

At low temperature (5°C), the results in Figure 8*a* illustrated that transverse strains at the top of pavement were positive outside of the loading area. However, the maximum transverse tensile strain had a very small magnitude and occurred just outside of tire edge (at distances of 4.9 cm). The critical tensile strain value at the bottom of AC layer was larger than that at the top, which inferred that crack might initiate at the bottom of AC layer. Compared to the horizontal strains at 5°C, Figures 8(*b* and *c*) depicted that, due to the time-temperature dependency of asphalt materials at elevated temperatures (25°C and 50°C), transverse strain at the pavement surface increased significantly, especially at the locations near to the tire edges. This finding was more evident at 50°C, which the pavement susceptibility to TDC increased. As shown in Figure 8*c*, the maximum horizontal tensile strain at the bottom was insignificant, while it reached nearly 500 microstrains at the top. The calculated results led to an important finding that the surface tensile strain developed at high and medium temperatures was the primary cause of TDC, which was in agreement with micro-mechanic approach and discrete element simulations (Wang et al., 2003). In addition, the laboratory tests and FEM analysis results in another study demonstrated that once the temperature increases, TDC may initiate due to the contribution of ruts (De Freitas et al., 2005).

To investigate the AC layer thickness effect on horizontal strains through viscoelastic analysis, three AC thicknesses, including 10, 20 and 30 cm, were analyzed and the critical responses were presented in Table 3, where the results of the elastic analysis from a previous study were also shown as a comparison (Zhao et al., 2018). It should be noted that the equivalent elastic modulus was used for the AC layer in the elastic analysis. As the depth of AC layer increased from 10 to 30 cm, the maximum tensile strain at the bottom decreased at low temperature, while the critical tensile strains at pavement surface increased at the medium and high temperatures. Despite relatively small magnitudes of tensile strain at bottom of AC layer, cracking may initiate in CTB layer, and then reflective cracking propagates into the AC layer.

Comparison of the viscoelastic and elastic analyses results in Table 3 showed that the critical horizontal strains at medium and high temperatures had larger values in the viscoelastic analysis because of the time-temperature dependent properties of HMA mixtures. The critical transverse tensile strain leads to cracking at pavement surface and in a longitudinal direction, which agrees with the typical TDC pattern in the field (ARA, 2004). These figures provided a practical tool in new pavement design to avoid the consideration of fatigue cracking only at the bottom of AC layer at different temperatures. In addition, utilizing viscoelastic analysis had a significant effect on the magnitude of the critical tensile strain at the AC surface.

3.1.2. Pavements with Granular Base

In order to explore the possibility of TDC initiation in pavements with GB, the horizontal strains were calculated at temperatures 5, 25, and 50°C and the response profiles were presented in Figures 9(*a, b,* and *c*), respectively. It was observed that at low and medium temperatures, the maximum transverse strain at the top of AC layer was in tension; however, this small magnitude had an insufficient influence on TDC initiation. In contrast, longitudinal strain induced at the bottom of AC layer causes bottom-up cracking to be a dominant type of fatigue cracking. When the temperature varied from 25 to 50°C, the maximum transverse strain at surface increased from 11.5 microstrains to 411.3 microstrains and longitudinal strain at the AC layer bottom changed from 71.3 microstrains to 187.3 microstrains. Since the rate of increase in strain responses at the surface was much faster than that at the bottom, it was expected that TDC to occur in hot weather circumstances. To evaluate the effect of asphalt layer thickness on TDC, horizontal strains responses were computed as summarized in Table 4.

Viscoelastic analysis results in the table showed that the critical tensile strain locations and directions for AC thicknesses of 10 and 20 cm were similar to 30 cm thickness at temperatures analyzed. Also, at high temperatures, the viscoelastic properties of asphalt layers caused the transverse strains to arise at the top of AC layers with different thicknesses; while in the elastic analysis, transverse strain was critical only for a thick AC layer (30 cm) at temperature of 50°C. The viscoelastic analysis results for the pavement with CTB and GB revealed that possibility of TDC initiation was greatly induced by increasing temperature and AC thickness variations. Furthermore, larger horizontal strain values obtained from viscoelastic analysis compared to elastic analysis justifies the importance of accurate mechanistic characterization of pavement structure.

3.1.3. Effect of Tire-Pavement Stress Distribution

To investigate the influence of magnitude and direction of the contact stress on TDC in asphalt pavement, three contact traction components (vertical, transverse, and longitudinal) and tire pressures of 0.55, 0.7 and 0.85 MPa were considered in the analyses. According to the experimental measurements conducted by Al-Qadi et al. (2008), magnitudes of transverse and longitudinal contact stresses ranged from 11-34% of the maximum vertical stress. Considering contact stresses in three directions, analyses were carried out at temperature 50°C and a constant vehicle speed of 8 km/h as the most critical condition for TDC. As shown in Figure 10, the magnitude of maximum transverse strain increased with increasing the tire pressure, demonstrating that the potential of TDC intensifies with increasing tire pressure. Changing the tire pressure from 0.7 to 0.85 MPa were resulted in 21-28% increase of transverse strain magnitudes at different AC thicknesses, while the reduction of tire pressure from 0.7 to 0.55 MPa caused the transverse strain magnitudes to decline 10-18% at the pavement surface.

Furthermore, a comparison of maximum transverse strain at the surface under vertical contact stress with that obtained under 3D contact stresses was presented at Table 5. The results revealed that utilizing the contact stress distribution in three directions, increased transverse strain value 48-55% greater at different AC thicknesses. This finding indicates that considering tire-pavement stress distributions would increase severity of TDC and reduce the service life of pavement structures.

3.2. Moving Load Effect on Horizontal Strains

To investigate the likelihood of TDC initiation in pavement structure subjected to moving loads, the horizontal strains responses induced by passage of dual tire loads at three different speeds, namely 8, 48, and 96 km/h, were computed for the pavement structures shown in Table 2 at low, medium and high temperatures. The vertical stresses of the moving load under the center of one tire in a dual tire assembly were depicted in Figure 11. As anticipated, by increasing AC layer depths below the surface, the vertical stress magnitudes were dissipated, whereas the pulse durations of vertical stress rose with depth. This observation is mainly important for calculating the asphalt layer responses, which have time-dependent properties.

To illustrate the variations of critical horizontal strains at a low speed (8km/h), the response curve of thick pavement with CTB layer was compared to that with GB layer. Figures 12 showed the critical transverse strains at the top of pavements with CTB and GB layers at a temperature of 50°C. It was observed from the figure that in thick pavement with CTB layer, the maximum transverse strain increased greater than that in pavement with GB. Because of the viscoelastic effects in AC layer, the response curves were not symmetric. The wheels reached the top of analysis point at 4m traveling distance, which was shown in the figure as a vertical line. As seen, the peak strains occurred after the wheels left the analysis point. The shapes of the response curves were identical to those measured from pavement sections in the field (Al-Qadi and Wang, 2009; Elseifi et al., 2006).

The viscoelastic analysis of moving load at three vehicle speeds (8, 48, and 96 km/h) was carried out efficiently, and critical horizontal strains at AC layers were presented in Figures 13(*a* and *b*) for the pavements with CTB and GB layers respectively. The figures illustrated that the transverse strain at surface was affected strongly by the moving load speeds and increased its magnitude when the vehicle speeds decreased. In addition, a comparison of responses at different speeds demonstrated that possibility of TDC in pavements with CTB was higher than that in pavements with GB.

However, variations of AC thicknesses had an inadequate effect on the critical transverse strains at high temperature; vehicle speed impact on transverse strains was remarkable. As an example, in thick AC layer, once the vehicle speed decreased from 96 to 8 km/h, the transverse strains increased approximately 3.1 and 5.1 times in magnitudes for the pavements with CTB and GB, respectively. This finding revealed that at high temperature, the rate of increase in transverse strain for the pavement with GB is much faster compared to the pavement with CTB, which may lead to major structural failures on the pavement surface at a low speed.

At medium temperature (25°C), the critical horizontal strains in AC layer with 30 cm thickness were calculated at a low speed moving load, and the response profiles were plotted in Figure 14. The critical tensile strain at the surface occurred in transverse direction for the pavement with CTB, while the longitudinal strain at the bottom was critical for the pavement with GB. The horizontal strain curves at the top and bottom of AC layer were composed of the compressive part followed by a tensile part and another compressive part. To identify the critical horizontal strain locations and directions in the asphalt layer with different thicknesses and vehicle speeds, significant analyses were carried out and results were depicted in 15(*a* and *b*) for the pavements with CTB and GB, respectively.

However, horizontal strains were affected noticeably by vehicle speeds and AC thicknesses; these factors' influence on responses was relatively different in pavements with CTB and GB. Unlike the insignificant effect of asphalt thickness on horizontal strains at 50°C, it was realized that by increasing the AC thicknesses at temperature of 25°C, the transverse strains at pavement surface became larger for the pavements with CTB, whereas the opposite trends were obtained for longitudinal strains at the bottom of asphalt layers in the pavements with GB. In pavements with thick AC layers, the speeds reductions had little effect on longitudinal strains at the bottom, while the rate of increase in transverse strain value at the top was significant. In contrast, in thin AC layer, decreasing the vehicle speeds caused the longitudinal strains at the bottom to increase more than transverse strain at the top. This observation causes the bottom-up cracking to be a dominant type of fatigue cracking in pavements with GB at medium temperature.

At a low temperature (5°C), critical responses of pavements with CTB and GB subjected to moving loads were presented in Figures 16. It was seen that the longitudinal strain was the critical horizontal response at 5°C, and the peak value arose when the moving loads left the analysis point at 4m traveling distance. However, the calculated longitudinal strain curves were asymmetric at the analysis point in which demonstrating viscoelastic behavior of asphalt layer, the results showed that viscoelasticity effect was insignificant at low temperature. In addition, due to strong support from the CTB layer and low viscoelastic effect in AC layers, the critical longitudinal strains were small in magnitudes. From the results obtained, it was found that bottom-up cracking was the dominant type of fatigue cracking at low temperature.

Although, the locations and directions of the critical horizontal strains calculated from stationary and moving loads were similar at different temperatures, the values obtained from the analysis of moving loads were slightly smaller. This finding was consistent with the lateral stress results measured in the field (Assogba et al. 2019).

4. Summary and Findings

In this study, the viscoelastic responses of multilayered pavement structures were analyzed to improve the understanding of top-down fatigue cracking mechanism. The EVECP solution was employed to solve the viscoelastic step response function of pavement. Utilizing the Lucas algorithm and then integration, summation, and then extrapolation method, the irregular oscillation behavior of surface response converged to irregular oscillation. Sensitivity analyses were conducted to investigate the effect of temperatures, vehicle speeds and AC thicknesses on TDC, by computing the maximum horizontal strains at the top of pavements. Analyses were performed on the pavements with CTB and GB under stationary and moving loads. The main findings of this study are summarized below:

- According to the maximum transverse strains calculated at a very close distance to tire edge, high temperature and low vehicle speed were among the predominant factors contributing TDC.
- Since the critical response and location of TDC were consistent with the elastic analysis results, the procedure adopted in this study could accurately determine the viscoelastic response at pavement surface and provided an effective tool for pavement structure analysis and design. However, critical strains calculated from viscoelastic analysis have larger values at high temperature due to the time and temperature dependency of AC material.
- Based on the critical responses obtained from stationary and moving loads, a thick AC layer has a pivotal role in crack initiation at the surface compared to the thin AC layer.
- The likelihood of TDC at higher temperatures increases in pavements with CTB and GB, whereas the pavements become more vulnerable to bottom-up cracking at medium and low temperature.
- The moving load analysis results at high temperature illustrated that a decrease in

vehicle speed increased maximum transverse strain at the top of AC layer, which causes the pavement surface to become vulnerable to TDC. Furthermore, rate of increase in transverse strain for the pavements with GB was much faster compared to the pavements with CTB, which may lead to major structural failures on the pavement surface at a low speed.

- At low temperature, utilizing pavements with CTB layer diminished the longitudinal strains at the bottom of AC layers due to the strong support from the base layer. Thus, it can be considered as a solution against bottom-up cracking.

The surface viscoelastic analysis results of this research provided beneficial insight to pavement design. However, the proposed approach needs development to consider actual non-uniform distributed tire-pavement contact stresses.

Acknowledgments

This research was sponsored by National Natural Science Foundation of China (51678114), Urumqi Transportation Research Project (JSKJ201806), Inner Mongolia Transportation Research Project (NJ-2014-21, NJ-2015-36), and Shanxi Transportation Research Project (2015-1-22). The authors gratefully acknowledge their financial support.

References

Alae, M., Haghshenas, H. F., & Zhao, Y. (2019). Evaluation of top-down crack propagation in asphalt pavement under dual tire loading. Canadian Journal of Civil Engineering, 46(8), 704-711.

Alae, M., Zhao, Y., Zarei, S., Fu, G., & Cao, D. (2020). Effects of layer interface conditions on top-down fatigue cracking of asphalt pavements. International Journal of Pavement Engineering, 21(3), 280-288.

Al-Qadi, I. L., & Wang, H. (2009). Full-depth pavement responses under various tire configurations: Accelerated pavement testing and finite element modeling. Journal of the Association of Asphalt Paving Technologists, 78, 721-760.

Al-Qadi, I. L., Wang, H., Yoo, P. J., & Dessouky, S. H. (2008). Dynamic analysis and in situ validation of perpetual pavement response to vehicular loading. Transportation research record, 2087(1), 29-39.

Applied Research Associates. (2004). Guide for mechanistic-empirical design of new and rehabilitated pavement structures. Final Report, National Cooperative Highway Research Program (NCHRP) Project 1-37A. Albuquerque, NM: National Research Council.

Asphalt Research Consortium. (2013). Report J: Pavement Response Model to Dynamic Loads 3D Move. Quarterly Technical Progress Report, Asphalt Research Consortium, USA.

Archilla, A. R. (2015). Top-Down fatigue Cracking in High-Temperature Environments. Transportation Research Record: Journal of the Transportation Research Board, (2507), 128-137.

Assogba, O. C., Tan, Y., Sun, Z., Lushinga, N., & Bin, Z. (2019). Effect of vehicle speed and overload on dynamic response of semi-rigid base asphalt pavement. Road Materials and Pavement Design, 1-31.

Burmister, D. M. (1945). The general theory of stresses and displacements in layered soil systems. II. Journal of Applied Physics, 16(3), 126-127.

Burmister, D. M. (1943). The theory of stress and displacements in layered systems and applications to the design of airport runways. Highway Research Board, Proceedings of 23rd Annual Meeting, 23, 126–144.

Chabot, A., Chupin, O., Deloffre, L., & Duhamel, D. (2010). Viscoroute 2.0 A: tool for the simulation of moving load effects on asphalt pavement. Road Materials and Pavement Design, 11(2), 227-250.

Chen, E. Y., Pan, E., & Green, R. (2009). Surface loading of a multilayered viscoelastic pavement: Semi-analytical solution. Journal of engineering mechanics, 135(6), 517-528.

De Freitas, E. F., Pereira, P., Picado–Santos, L., & Papagiannakis, A. T. (2005). Effect of construction quality, temperature, and rutting on initiation of top-down cracking. Transportation research record, 1929(1), 174-182.

Dinegdae, Y. H., & Birgisson, B. (2018). Effects of truck traffic on top-down fatigue cracking performance of flexible pavements using a new mechanics-based analysis framework. Road Materials and Pavement Design, 19(1), 182-200.

Dinegdae, Y. H., Onifade, I., Jelagin, D., & Birgisson, B. (2015). Mechanics-based top-down fatigue cracking initiation prediction framework for asphalt pavements. Road Materials and Pavement Design, 16(4), 907-927.

Dai, S. T., Van Deusen, D., Beer, M., Rettner, D., & Cochran, G. (1997). Investigation of flexible pavement response to truck speed and FWD load through instrumented pavements.

In 8th International Conference on Asphalt Pavements Federal Highway Administration.

Dubois, F., Moutou-Pitti, R., Picoux, B., & Petit, C. (2012). Finite element model for crack growth process in concrete bituminous. Advances in Engineering Software, 44(1), 35-43.

Elseifi, M. A., Al-Qadi, I. L., & Yoo, P. J. (2006). Viscoelastic modeling and field validation of flexible pavements. Journal of engineering mechanics, 132(2), 172-178.

Ferry, J.D. (1980). Viscoelastic properties of polymers, 3rd edition. John Willey & Sons., New York.

Gaver Jr, D. P. (1966). Observing stochastic processes, and approximate transform inversion. Operations Research, 14(3), 444-459.

Grellet, D., Doré, G., Chupin, O., & Piau, J. M. (2018). Highlighting of the viscoelastic behaviour of interfaces in asphalt pavements–a possible origin to top-down cracking. Road Materials and Pavement Design, 19(3), 581-590.

Groenendijk, J. (2000). Accelerated testing and surface cracking of asphaltic concrete pavements (Ph.D. dissertation). Delft University of Technology.

Gu, F., Luo, X., West, R. C., Taylor, A. J., & Moore, N. D. (2018). Energy-based crack initiation model for load-related top-down cracking in asphalt pavement. Construction and Building Materials, 159, 587-597.

Guo, S., Fan, X., Gao, K., & Li, H. (2020). Precision controllable Gaver–Wynn–Rho algorithm in Laplace transform triple reciprocity boundary element method for three-dimensional transient heat conduction problems. Engineering Analysis with Boundary Elements, 114, 166-177.

Haddad, Y. M. (1995). Viscoelasticity of engineering materials, Chapman & Hall, New York.

Huang, Y. (2003). Pavement analysis and design. Prentice Hall, Englewood Cliffs, New Jersey.

Khazanovich, L., & Wang, Q. (2007). MnLayer: high-performance layered elastic analysis program. Transportation Research Record, 2037(1), 63-75.

Ling, M., Luo, X., Chen, Y., Hu, S., & Lytton, R. L. (2019). A calibrated mechanics-based model for top-down cracking of asphalt pavements. Construction and Building Materials, 208, 102-112.

Ling, M., Luo, X., Chen, Y., Gu, F., & Lytton, R. L. (2020). Mechanistic-empirical models for top-down cracking initiation of asphalt pavements. International Journal of Pavement Engineering, 21(4), 464-473.

Lucas, S. K., & Stone, H. A. (1995). Evaluating infinite integrals involving Bessel functions of arbitrary order. Journal of Computational and Applied Mathematics, 64(3), 217-231.

Maina, J., & Matsui, K. (2005). Elastic multi-layered analysis using DE-integration. Publications of the Research institute for Mathematical Sciences, 41(4), 853-867.

Myers, L. A., Roque, R., & Birgisson, B. (2001). Propagation mechanisms for surface-initiated longitudinal wheelpath cracks. Journal of the Transportation Research Board, 1778, 113–122.

Nilsson, R. N., Oost, I., & Hopman, P. C. (1996). Viscoelastic analysis of full-scale pavements: validation of VEROAD. Transportation research record, 1539(1), 81-87.

Qin, F., Yu, Y., & Rudolphi, T. (2010). Finite element modeling of viscoelastic stress analysis under moving loads. Int. J. Mech. Mater. Eng, 1(4), 226-233.

Rahman, A., Huang, H., Ai, C., Ding, H., Xin, C., & Lu, Y. (2019). Fatigue performance of interface bonding between asphalt pavement layers using four-point shear test set-up. International Journal of Fatigue, 121, 181-190.

Roque, R., Zou, J., Kim, Y. R., Baek, C., Thirunavukkarasu, S., Underwood, B. S., & Guddati, M. N. (2010). Top-down cracking of hot-mix asphalt layers: Models for initiation and propagation (No. NCHRP Project 1-42A).

Saad, B., Mitri, H., & Poorooshasb, H. (2005). Three-dimensional dynamic analysis of flexible conventional pavement foundation. Journal of transportation engineering, 131(6), 460-469.

Sangpetngam, B., Birgisson, B., & Roque, R. (2004). Multilayer boundary-element method for evaluating top-down cracking in hot-mix asphalt pavements. Transportation Research Record, 1896(1), 129–137.

Tschoegl, N. W. (1989). The phenomenological theory of linear viscoelastic behavior: An introduction, Springer, New York.

Valkó, P. P., & Abate, J. (2004). Comparison of sequence accelerators for the Gaver method of numerical Laplace transform inversion. Computers & Mathematics with Applications, 48(3-4), 629-636.

Wang, L. B., Myers, L. A., Mohammad, L. N., & Fu, Y. R. (2003). Micromechanics study on top-down cracking. Transportation Research Record, 1853(1), 121-133.

Wang, H., & Al-Qadi, I. L. (2010). Near-surface pavement failure under multiaxial stress state in thick asphalt pavement. Transportation research record, 2154(1), 91-99.

Wang, H. (2011). Analysis of tire-pavement interaction and pavement responses using a decoupled modeling approach (Doctoral Dissertation). University of Illinois at Urbana-Champaign.

Wang, H., Ozer, H., Al-Qadi, I. L., & Duarte, C. A. (2013). Analysis of near-surface cracking under critical loading conditions using uncracked and cracked pavement models. Journal of Transportation Engineering, 139(10), 992-1000.

Wu, S., & Muhunthan, B. (2019a). A mechanistic-empirical model for predicting top-down fatigue cracking in an asphalt pavement overlay. Road Materials and Pavement Design, 20(6), 1322-1353.

Wu, S., Wen, H., Zhang, W., Shen, S., Mohammad, L. N., Faheem, A., & Muhunthan, B. (2019b). Field performance of top-down fatigue cracking for warm mix asphalt pavements. International Journal of Pavement Engineering, 20(1), 33-43.

Zhao, Y., Alae, M., & Fu, G. (2018). Investigation of mechanisms of top-down fatigue cracking of asphalt pavement. Road Materials and Pavement Design, 19(6), 1436-1447.

Zhao, Y., Ni, Y., Wang, L., & Zeng, W. (2014). Viscoelastic response solutions of multilayered asphalt pavements. Journal of Engineering Mechanics, 140(10), 04014080.

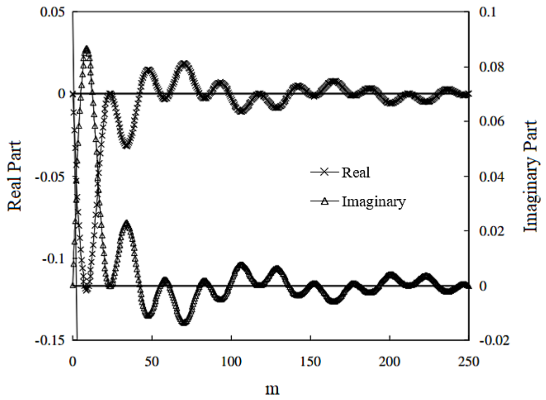

(a)

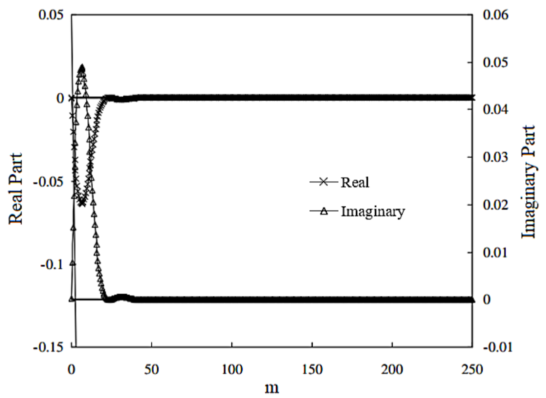

(b)

Figure 1. Variations of $\bar{F}(m,s)$ at: (a) Points A (pavement surface); (b) Point B (10 cm below the surface)

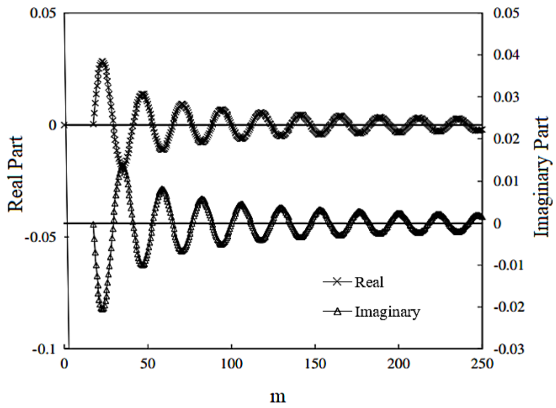

(a)

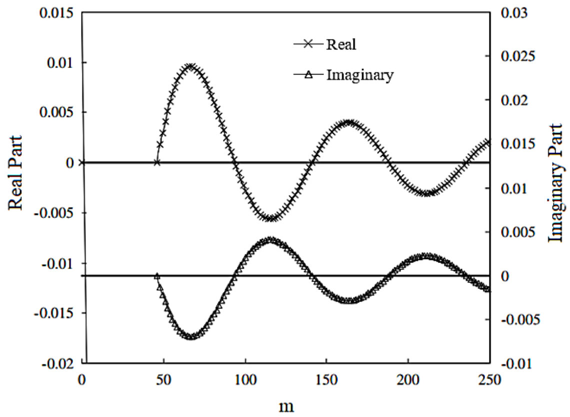

(b)

Figure 2. Variations of $\bar{F}(m,s)$ at Point A for: (a) high-frequency; (b) low-frequency component

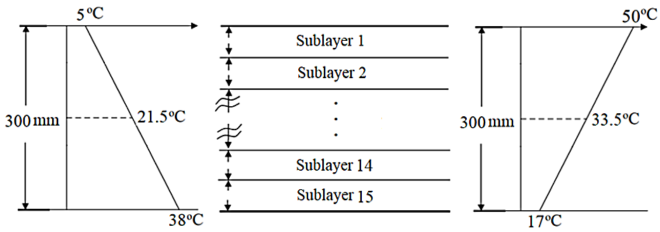

Figure 3. Illustration of different temperatures gradients within 30 cm AC layer depth

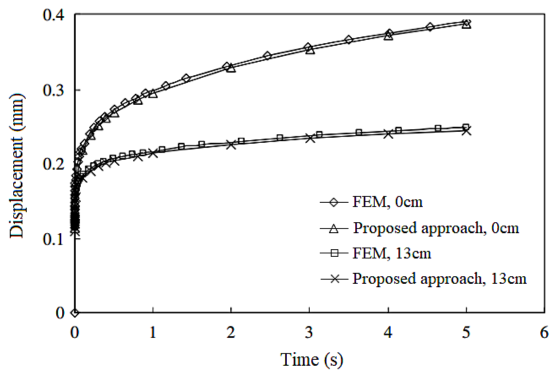

Figure 4. Comparison of displacements at the center of the tire and at a radial distance of 13 cm

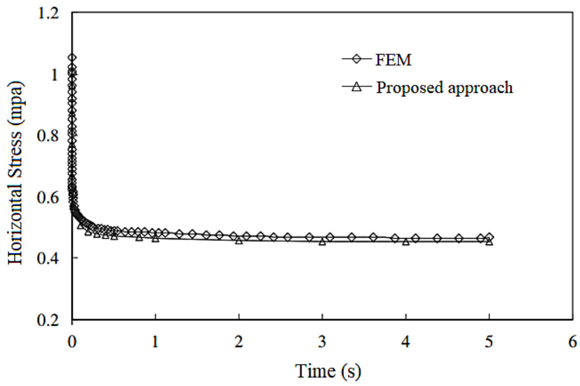

(a)

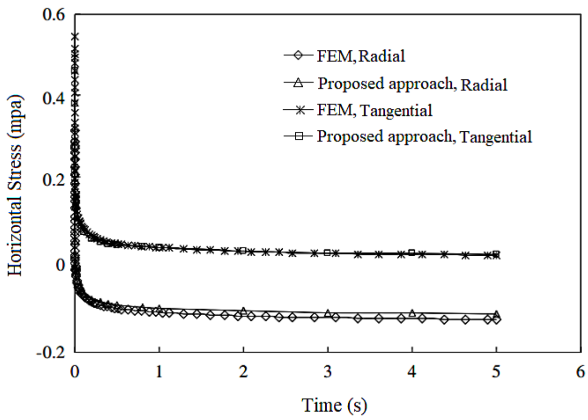

(b)

Figure 5. Comparison of horizontal stresses at: (a) the center of tire, and (b) a radial distance of 13 cm

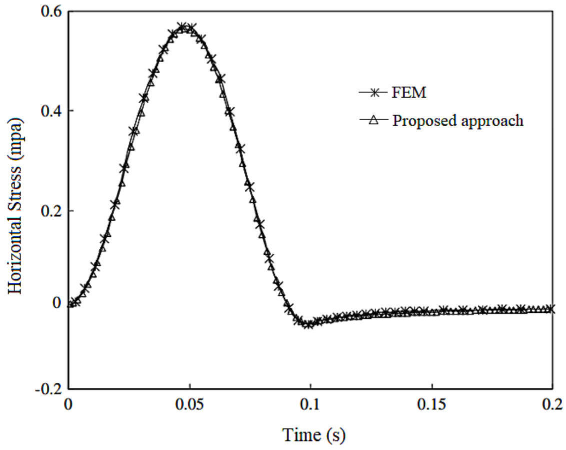

Figure 6. Comparison of horizontal stress at the center of the tire under haversine loading

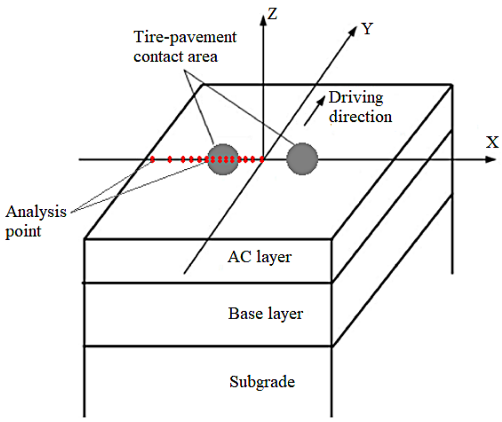

Figure 7. The sketch of 3D pavement structure with tire-pavement contact area and analysis points

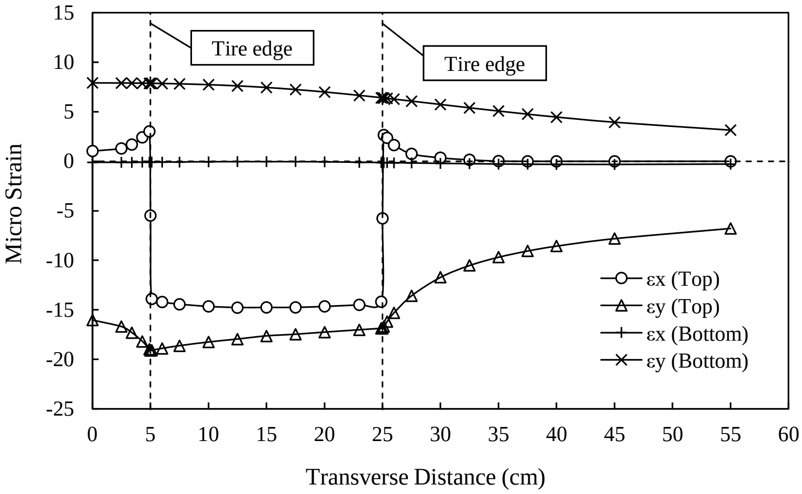

(a)

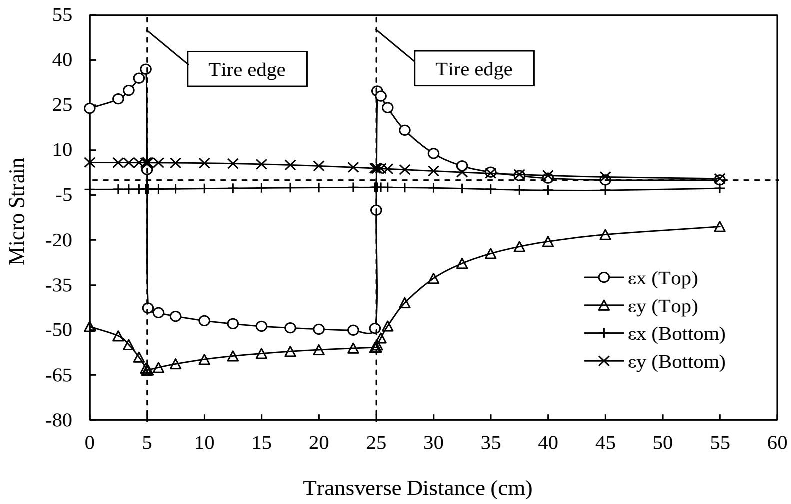

(b)

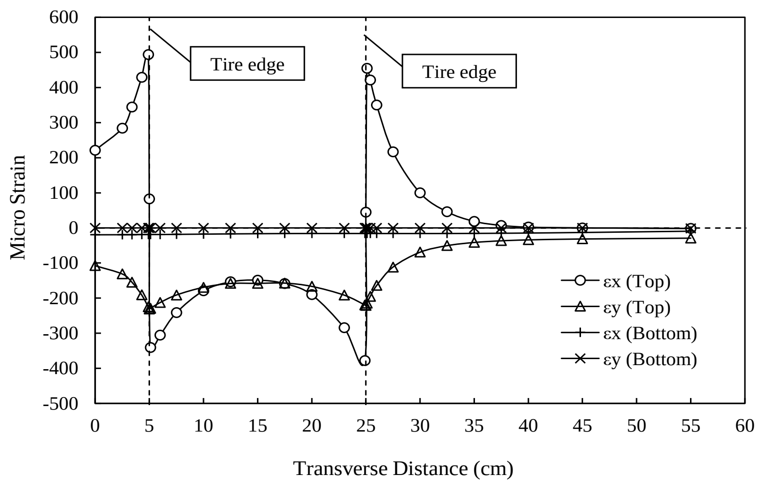

(c)

Figure 8. Horizontal strains at the top and bottom of thick AC layer with CTB at temperatures:

(a) 5°C, (b) 25°C, and (c) 50°C

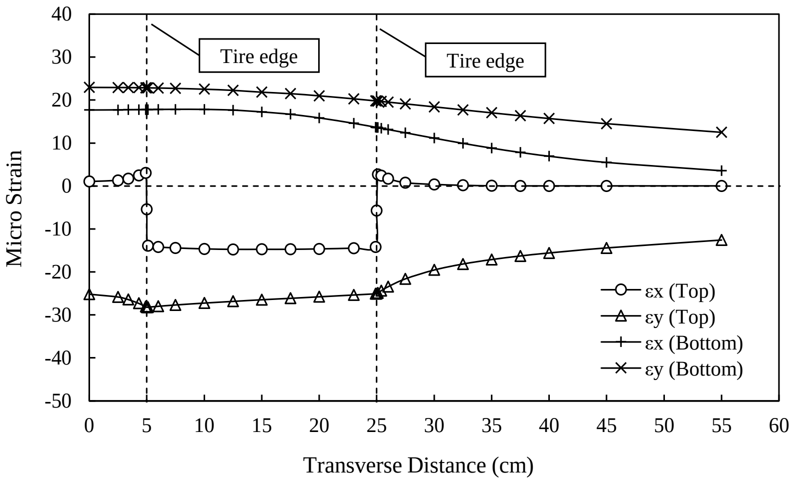

(a)

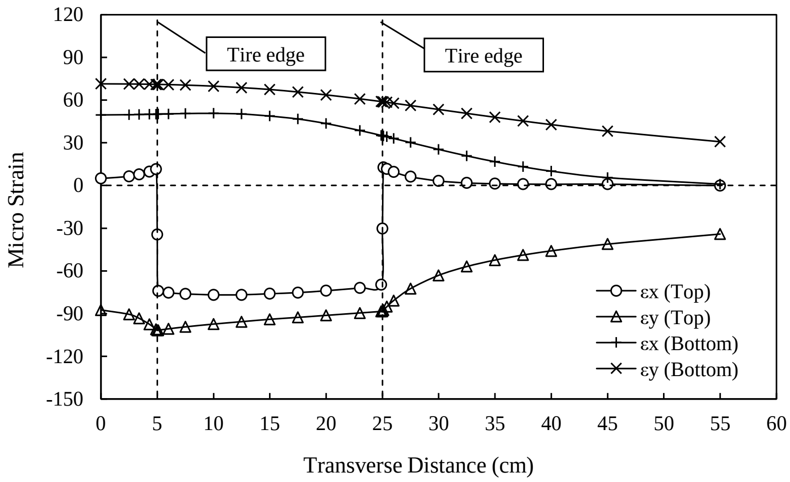

(b)

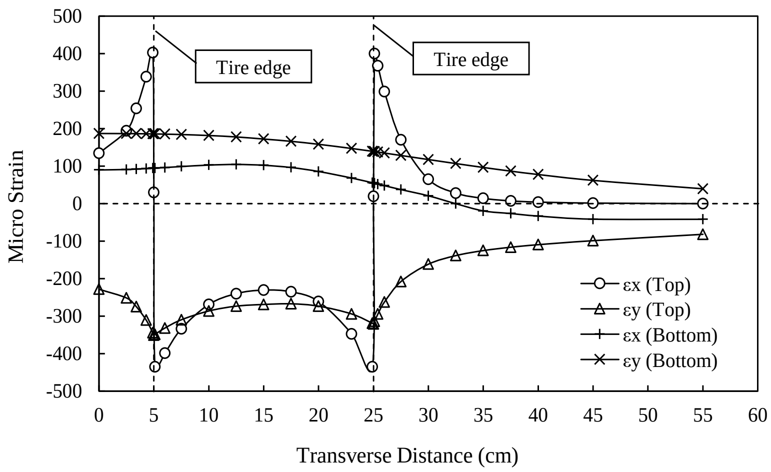

(c)

Figure 9. Horizontal strains at the top and bottom of thick AC layer with GB at temperatures:

(a) 5°C, (b) 25°C, and (c) 50°C

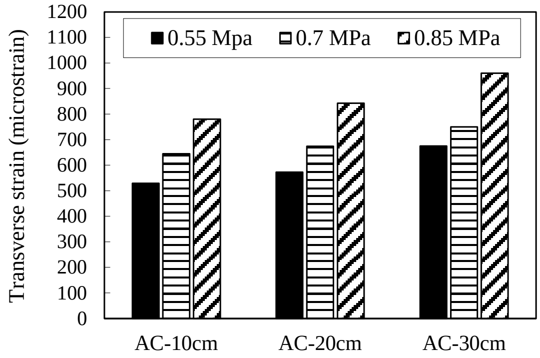

Figure 10. Effect of tire tire-pavement stresses on transverse strain at the pavement surface

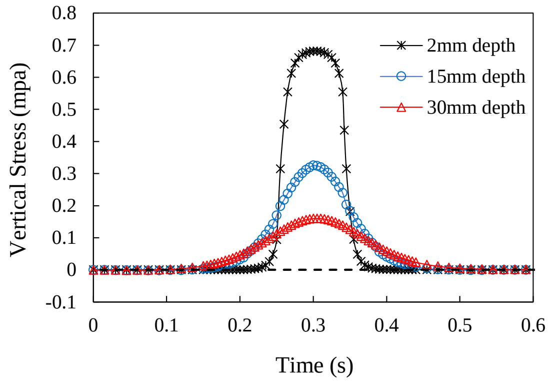

Figure 11. Vertical stress pulses under a moving load at different depths and temperature 50°C

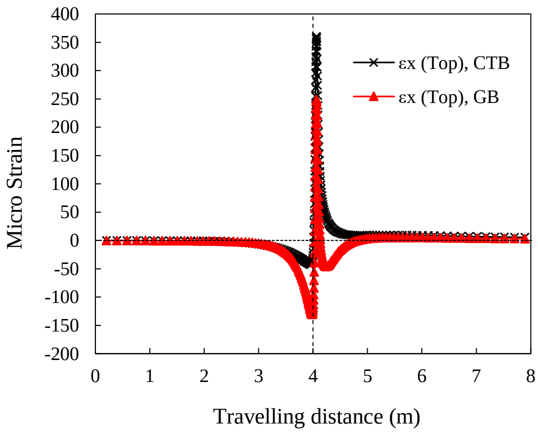

Figure 12. Critical horizontal strains at pavements with different base layers (AC-30 cm, temperature 50°C, speed 8km/h)

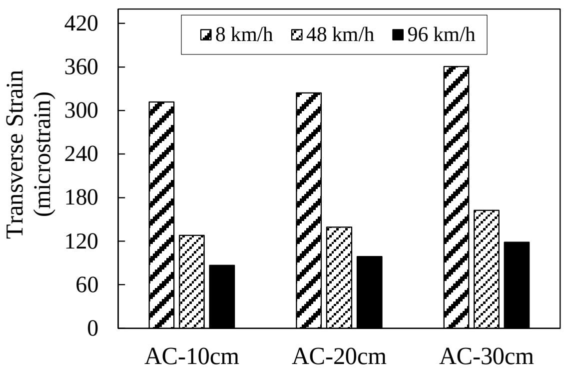

(a)

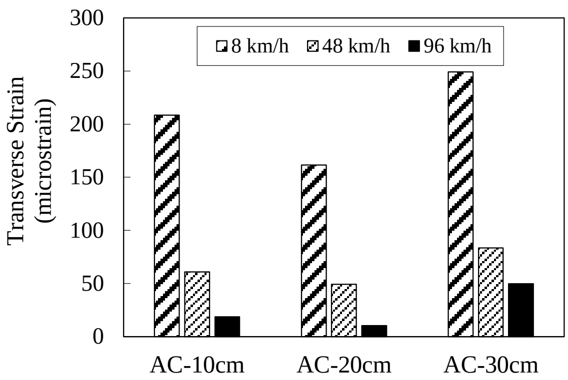

(b)

Figure 13. Influence of vehicle speeds on critical horizontal strains at temperature of 50°C for pavements with: (a) CTB, and (b) GB layers

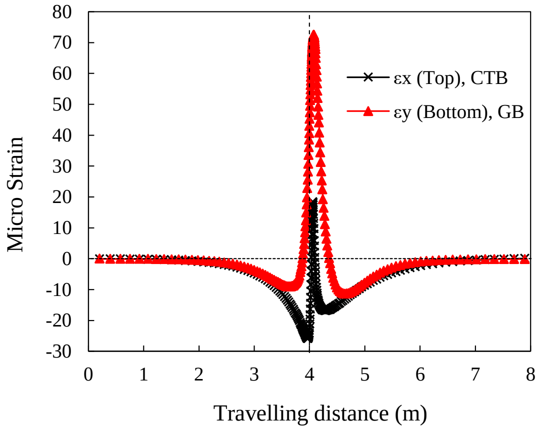

Figure 14. Critical horizontal strains at pavements with different base layers (AC-30 cm, temperature 25°C, speed 8km/h)

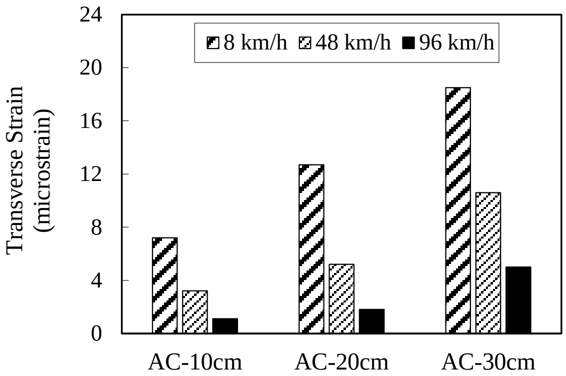

(a)

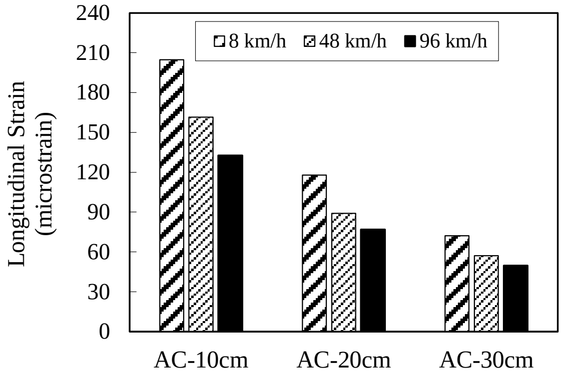

(b)

Figure 15. Influence of vehicle speeds on critical horizontal strains at temperature of 25°C for pavements with: (a) CTB, and (b) GB layers

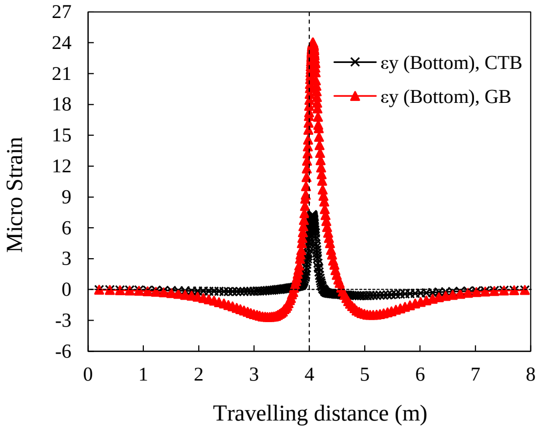

Figure 16. Critical horizontal strains at pavements with different base layers (AC-30 cm, temperature 5°C, speed 8km/h)

Table 1. Coefficients of MHN model

Mix type	E^*_∞ (MPa)	E^*_0 (MPa)	α	β	ω_0	C_1	C_2
AC20	32128	104.8	0.257	1.733	407.9	15.3	139.0

Table 2. Pavement structure parameters used in analyses

Layer	Thickness (cm)	Modulus (MPa)	Poisson's ratio
HMA	10, 20, 30	Viscoelastic	0.3
Base	30	280 (GB)	0.35
		7000 (CTB)	0.25
Subgrade	-	60	0.4

Table 3. Critical tensile strains and locations for pavement with CTB

AC thickness (cm)	Temperature (°C)	Critical location (LVEA*)	Direction	Value (με) (LVEA*)	Value (με) (LEA**)
10	5	Bottom	Longitudinal	12.8	12.0
	25	Top	Transverse	21.6	10.2
	50	Top	Transverse	435.8	331.7
20	5	Bottom	Longitudinal	10.6	9.9
	25	Top	Transverse	32.5	19.4
	50	Top	Transverse	446.4	391.4
30	5	Bottom	Longitudinal	7.8	7.4
	25	Top	Transverse	36.9	24.2
	50	Top	Transverse	483.8	385.4

*LVEA= linear viscoelastic analysis
**LEA= linear elastic analysis

Table 4. Critical tensile strains and locations for pavement with GB

AC thickness (cm)	Temperature (℃)	Critical location (LVEA*)	Direction-Value (με) (LVEA*)		Direction-Value (με) (LEA**)	
10	5	Bottom	Longitudinal	100.6	Longitudinal	90.5
	25	Bottom	Longitudinal	237.1	Longitudinal	200.2
	50	Top	Transverse	381.7	Longitudinal	386.5
20	5	Bottom	Longitudinal	41.9	Longitudinal	37.4
	25	Bottom	Longitudinal	120.7	Longitudinal	97.7
	50	Top	Transverse	325.6	Longitudinal	255.8
30	5	Bottom	Longitudinal	22.9	Longitudinal	20.1
	25	Bottom	Longitudinal	71.3	Longitudinal	56.6
	50	Top	Transverse	411.3	Transverse	284.8

*LVEA= linear viscoelastic analysis
**LEA= linear elastic analysis

Table 5. Comparison of maximum transverse strain at the surface under vertical stress and 3D contact stresses

Critical response (με)	Thickness (cm)	Loading condition	
		Vertical stress	3D Contact stresses
Transverse tensile strain	10	435.8	644.9
	20	446.4	674.1
	30	483.8	749.9